

Label-Free Coherent Anti-Stokes Raman Scattering Imaging of Coexisting Lipid Domains in Single Bilayers

Li Li[†] and Ji-Xin Cheng*

Weldon School of Biomedical Engineering and Department of Chemistry, Purdue University, West Lafayette, Indiana 47907

Received: December 6, 2007; In Final Form: January 4, 2008

Laser-scanning coherent anti-Stokes Raman scattering (CARS) microscopy was used to image lipid domains in single bilayers without any labeling. On the basis of the molecular packing density difference between liquid-disordered (L_d), liquid-ordered (L_o), and gel (S_o) phases, clear vibrational contrasts were generated between coexisting domains in a single bilayer of DOPC/DPPC (1:1) and DOPC/DPPC/cholesterol (4:4:2). The method reported here can be potentially applied to study phase segregation in live cell membranes which are highly heterogeneous and dynamic.

Introduction

Our understanding of membrane organization has been greatly advanced by various microscopy techniques. Fluorescence microscopy has been widely used for visualizing domains in model and cellular membranes with the aid of various probes that preferentially partition into specific phases. Atomic force microscopy offers morphological imaging with nanoscale resolution. Chemical imaging of membranes under physiological conditions has been realized based on the recent development of coherent anti-Stokes Raman scattering (CARS) microscopy.^{1–3} CARS is a four-wave mixing process in which the interaction of a pump field $E_p(\omega_p)$ and a Stokes field $E_s(\omega_s)$ with a sample generates an anti-Stokes field E_{as} at the frequency $\omega_{as} = 2\omega_p - \omega_s$.⁴ CARS microscopy permits molecular imaging based on molecular vibration spectroscopy, avoiding fluorophore labeling which may vary the properties of the sample. High-speed vibrational imaging has been realized using a laser-scanning CARS microscope with simultaneous forward and backward detection.⁵ The CARS signal is a coherent addition of the radiation from vibrational oscillators, making CARS microscopy a sensitive probe of the high-density CH_2 groups in a lipid bilayer. Wurpel et al. were able to acquire CARS spectra from single lipid monolayers and bilayers.⁶ Potma et al. have visualized phase segregation in giant unilamellar vesicle (GUV) bilayers composed of a binary mixture of nondeuterated and deuterated lipids.⁷ Li et al. demonstrated quantitative imaging of lipid partition into different domains on a supported bilayer using deuterated lipids.⁸ The deuterium labeling of lipid hydrocarbon chains creates the CD_2 stretch band at around 2090 cm^{-1} , well separated from the CH_2 stretch band at around 2850 cm^{-1} . However, the deuterium labeling cannot be applied to the study of cell membranes for which the composition is highly heterogeneous and dynamic. Therefore, it is important to visualize membrane domains in their natural state.

In this paper, we report a method that permits vibrational imaging of lipid domains without any labeling. It is known that a bilayer composed of a high- T_m and a low- T_m phospholipid can segregate into coexisting gel and liquid-disordered (L_d) phases at room temperature.⁹ The addition of cholesterol results in a new phase called the liquid-ordered (L_o) phase.¹⁰ Our strategy is based on the different lipid packing densities in the S_o , L_o , and L_d thermodynamic states. For example, the area per molecule is 47.2 \AA^2 for gel phase dimyristoylphosphatidylcholine (DMPC) at $10\text{ }^\circ\text{C}$ and 74.3 \AA^2 for liquid crystalline phase dioleoylphosphatidylcholine (DOPC) at $25\text{ }^\circ\text{C}$, indicating a much higher packing density in the gel phase than that in the L_d phase.^{11,12} To form macroscopic lipid domains, we prepared GUVs using the electroformation method.¹³ To avoid the lateral motion of domains inside of the bilayer and the undulation motion of the GUVs, we ruptured the GUVs on a coverslip, forming planar bilayer patches with static domains.¹⁴ The planar geometry and high stability of the supported bilayer facilitates CARS imaging at different Raman shifts and data analysis. Epidetection was used to suppress the nonresonant background from water and the glass. In this paper, we demonstrate that CARS microscopy is able to visualize coexisting domains with a high contrast based on the lipid packing difference.

Experimental Section

Materials. DOPC (1,2-dioleoyl-*sn*-glycero-3-phosphocholine), DPPC (1,2-dipalmitoyl-*sn*-glycero-3-phosphocholine), and cholesterol were purchased from Avanti Polar Lipids (Alabaster, AL) and used without further purification. BODIPY FL C5-HPC [2-(BODIPY-3-pentanoyl)-1-hexadecanoyl-*sn*-glycero-3-phosphocholine] was purchased from Invitrogen (Carlsbad, CA). The chain melting temperature (T_m) of DOPC and DPPC is -20 and $42\text{ }^\circ\text{C}$, respectively.

Preparation of Supported Homogeneous Bilayers. Homogeneous DOPC supported bilayers were prepared on cleaned coverslips by the fusion of small unilamellar vesicles.¹⁵ Details of the preparation procedure can be found elsewhere.⁸

* To whom correspondence should be addressed. Tel: 765 494 4335. Fax: 765 494 1193. E-mail: jcheng@purdue.edu.

[†] E-mail: li7@purdue.edu.

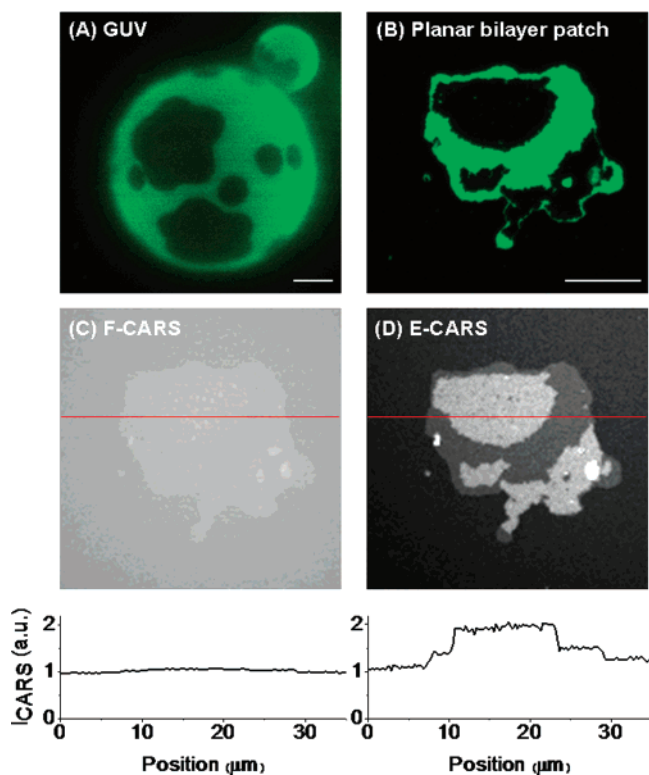


Figure 1. (A) Fluorescence image of 1:1 DOPC/DPPC GUVs labeled with 0.4% BODIPY PC. GUVs were prepared at 50 °C by the electroformation method and cooled to room temperature. (B) Fluorescence image of a bilayer patch of a 1:1 mixture of DOPC and DPPC. (C and D) F- and E-CARS images of the bilayer patch shown in (B). The intensity profiles along the red lines are shown below the images. The peak emission wavelength of BODIPY PC at 510 nm is spectrally separated from the CARS wavelengths at around 600 nm. The BODIPY PC probe was quickly bleached by the picosecond excitation beams and did not contribute to any contrast in the CARS images. The CARS images were an average of 40 frames. The acquisition time was 0.44 s for each frame of 256×256 pixels. The pump and Stokes powers at the sample were 3.0 and 1.4 mW, respectively. The same parameters were used for CARS imaging in other figures. No photodamage of the bilayer was observed. Bar = 10 μm .

Preparation of Giant Unilamellar Vesicles (GUVs) and Planar Bilayer Patches. GUVs of different lipid compositions were prepared on polydimethylsiloxane (PDMS)-chambered and indium tin oxide coated coverglasses by the electroformation method.¹³ To make bilayer patches, the GUV solution was mixed with an equal amount of the HEPES buffer (100 mM NaCl) and then deposited onto a cleaned coverslip. After at least 1 h of incubation at room temperature, the adjacent GUVs were fused and then ruptured onto the coverslip to form planar bilayer patches.¹⁴

CARS Imaging. Two collinearly combined 2.5 ps pulse trains at frequencies ω_p and ω_s were generated from two synchronized Ti:sapphire oscillators (Coherent Inc, Mira 900). A Pockels' cell (Conoptics, #350–160) was used to lower the repetition rate to 3.8 MHz. CARS images were acquired by raster scanning the two laser beams using a confocal microscope (Olympus, FV300/IX70). A water immersion objective with a 1.2 numerical aperture (NA) was used to focus the laser beams into the sample. The forward and backward CARS signals were collected by an air condenser (NA = 0.55) and the water objective, respectively, and were simultaneously detected by two photomultipliers (Hamamatsu, R3896 and H7422-40). The confocal pinhole was not used for CARS imaging, which has a lateral resolution of 0.23 μm and an axial resolution of 0.75 μm .⁵

Fluorescence Imaging. In order to correlate the CARS images with the membrane phases, we labeled the bilayers with the BODIPY PC probe that preferentially partitions into the more disordered phase.¹⁶ The peak emission wavelength of the BODIPY PC probe at 510 nm is spectrally separated from the CARS wavelengths at around 600 nm. Laser-scanning fluorescence imaging was carried out on the same microscope. A 488 nm Ar^+ laser was used to excite the BODIPY PC probe. For each bilayer sample, a fluorescence image was acquired before the CARS images. The fluorescent probe was quickly bleached by the picosecond excitation pulses and did not contribute to any contrast in the CARS images.

Results and Discussion

We started with the DOPC and DPPC binary mixture for which the phase diagram had been determined by a fluorescence anisotropy study.⁹ The GUVs shown in Figure 1A were segregated into a S_o phase and a L_d phase.¹⁷ The L_d phase was labeled by the BODIPY PC probe.¹⁶ To verify that what we observed was due to phase segregation, a temperature control experiment was performed by using a home-built water bath chamber. The domains in the GUVs disappeared at 36 °C (data not shown), consistent with the phase diagram reported before.⁹ The GUVs were ruptured onto a glass coverslip to form bilayer patches. Figure 1B shows the fluorescence image of a bilayer patch with coexisting domains, where the L_d phase was labeled by BODIPY PC. Figure 1C and D show the F- and E-CARS images of the same bilayer patch. The pump and Stokes frequency difference, $\omega_p - \omega_s$, was tuned to the CH_2 symmetric stretch vibration band at 2840 cm^{-1} . The F-CARS signal (Figure 1C) was dominated by the nonresonant background from glass and water. The E-CARS image (Figure 1D) displayed a clear vibrational contrast because the nonresonant background from the surrounding medium was mostly canceled out by the destructive interference among the backward CARS fields.¹⁸ The S_o domain that was not labeled by the BODIPY PC probe produced a larger CARS signal than that of the L_d domain because of the compact packing of DPPC in the S_o phase, permitting visualization of phase segregation without any labeling.

Due to the refractive index mismatch between water and the glass coverslip, the forward CARS field generated from the glass is partially reflected and coherently mixed with the backward resonant CARS field from the bilayer.¹⁹ The CARS signal arises from the third-order susceptibility, $\chi^{(3)}$, of a material²⁰

$$\chi^{(3)} = \frac{nA}{\delta - i\Gamma} + \chi_{\text{nr}}^{(3)} \quad (1)$$

where δ represents the detuning, $\Omega - (\omega_p - \omega_s)$, Ω is the vibrational frequency, Γ is the half width at half-maximum of an isolated Raman line, A is a constant representing the Raman scattering strength, n is the number of oscillators with the vibrational frequency Ω , and χ_{nr} represents the nonresonant contribution and is a constant in the absence of electronic resonance.⁴

Our sample can be considered as a Raman scatterer surrounded by a medium that only contributes to the nonresonant background (χ_{nr}). Assuming that the nonresonant background from the scatterer (e.g., a lipid bilayer) is negligible compared to that from the surrounding medium, the CARS intensity can be written as

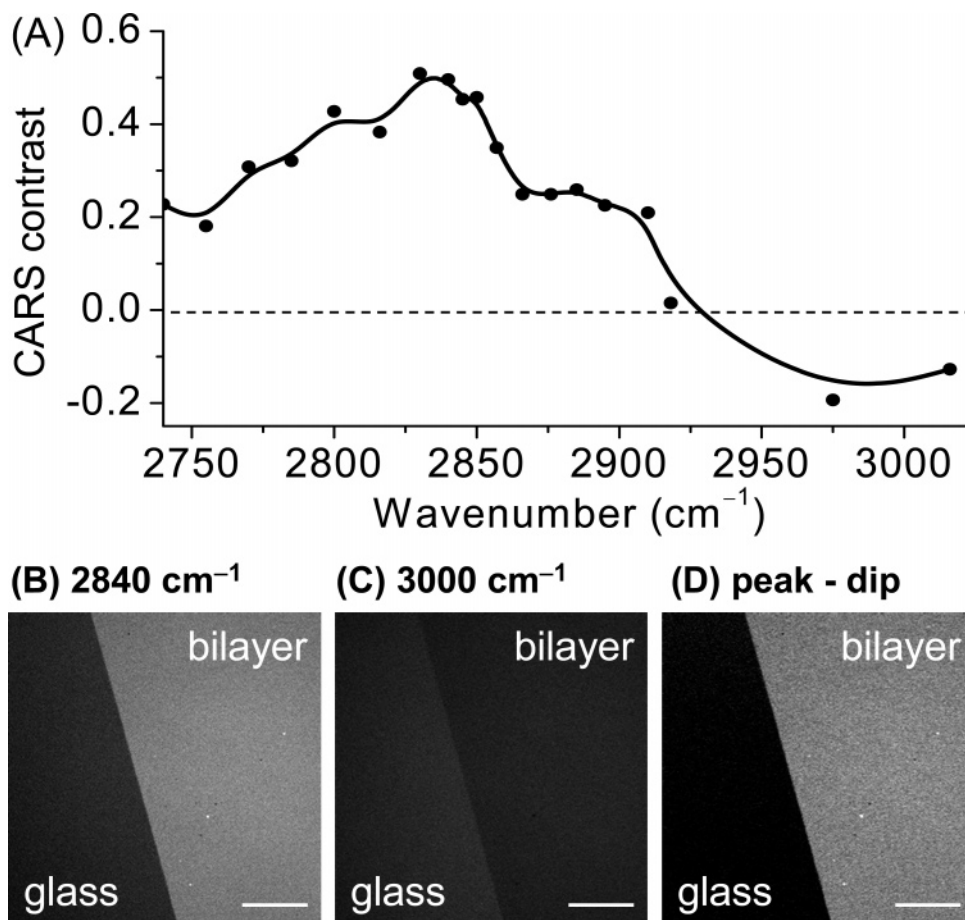


Figure 2. (A) CARS spectrum of a single DOPC bilayer obtained by manually tuning the Stokes frequency. The pump frequency was fixed at 14168 cm⁻¹. CARS images of a DOPC bilayer at peak (B) and dip (C) frequencies were shown below the spectrum. (D) The difference CARS images of the DOPC bilayer. Bar = 10 μm.

$$I_{\text{CARS}} \propto |\chi^{(3)}|^2 = \frac{n^2 A^2}{\delta^2 + \Gamma^2} + (\chi_{\text{nr}})^2 + \frac{2nA\chi_{\text{nr}}}{\delta^2 + \Gamma^2} \delta \quad (2)$$

The second item in the right side of eq 2 contributes to a constant background. The third term disperses the CARS spectral profile and results in a peak (ω_+) and dip (ω_-) at⁴

$$\omega_{\pm} = \Omega + \frac{1}{2} \left\{ \frac{nA}{\chi_{\text{nr}}} \pm \sqrt{\left(\frac{nA}{\chi_{\text{nr}}}\right)^2 + 4\Gamma^2} \right\} \quad (3)$$

The E-CARS spectrum of a supported DOPC bilayer was shown in Figure 2A. The Raman bands of symmetric and antisymmetric CH₂ and CH₃ stretch vibration bands reside in the 2700–3100 cm⁻¹ region. Due to the interference between the resonant signal from the bilayer and the back-reflected nonresonant background, the CARS peak for the symmetric CH₂ stretch appeared at 2840 cm⁻¹, red-shifted from its center vibration frequency at 2850 cm⁻¹. The antisymmetric CH₂ vibration and the CH₃ vibration canceled the dip of the symmetric CH₂ stretch band and created a new dip at around 3000 cm⁻¹. Accordingly, we observed a positive contrast from a DOPC bilayer at the peak (Figure 2B) and a negative contrast at the dip frequency (Figure 2C). The nonresonant background was removed by subtracting the image taken at 3000 cm⁻¹ (dip) from the image taken at 2840 cm⁻¹ (peak). In addition, the (peak – dip) signal (Figure 2D) contained a contribution from the interference between the resonant signal and the nonresonant background (the third item on the right side of eq 2), which increased the vibrational contrast.

The (peak – dip) CARS images for bilayers of pure DOPC/DPPC (1:1), DOPC/DPPC/cholesterol (4:4:2), and DOPC were shown in Figure 3. The intensity profiles of the lines were shown below the images. From the intensity profile in Figure 3A, the CARS contrast ratio is 3.73:1 between the DPPC-enriched S₀ and DOPC-enriched L_d domains of the current samples. The area per molecule for DPPC and DOPC at room temperature is 47.9 and 72.5 Å², respectively.²¹ Both DPPC and DOPC contain 28 CH₂ groups in one molecule. Thus, the density ratio of the CH₂ groups between the pure DPPC and the pure DOPC bilayer is 1.51. According to eq 2, the (peak – dip) intensity contains two contributions, one being quadratically and the other linearly proportional to the density of CH₂ groups. However, the observed CARS intensity ratio (3.73) is larger than the ratio of the squared CH₂ density (2.28). The orientation of CH₂ groups in lipid hydrocarbon chains might account for this result. In DOPC molecules, half of the hydrocarbon chain is tilted because of the C=C bond. Because the excitation polarization is parallel with the membrane surface, the CARS field from the tilted part is weaker. This polarization sensitivity increased the CARS contrast between DPPC and DOPC.

Adding 20% cholesterol to the 1:1 DOPC/DPPC mixture creates L₀ domains.¹⁷ The L₀ phase showed a positive CARS contrast compared to the L_d phase (Figure 3B), indicating that its packing density is higher than that of L_d. It was observed that the resonant CARS intensity from the L₀ phase was lower than that from the S₀ phase, whereas the CARS intensity from the L_d phase in the DOPC/DPPC/20% cholesterol bilayer was higher than that from the L_d phase in the DOPC/DPPC bilayer.

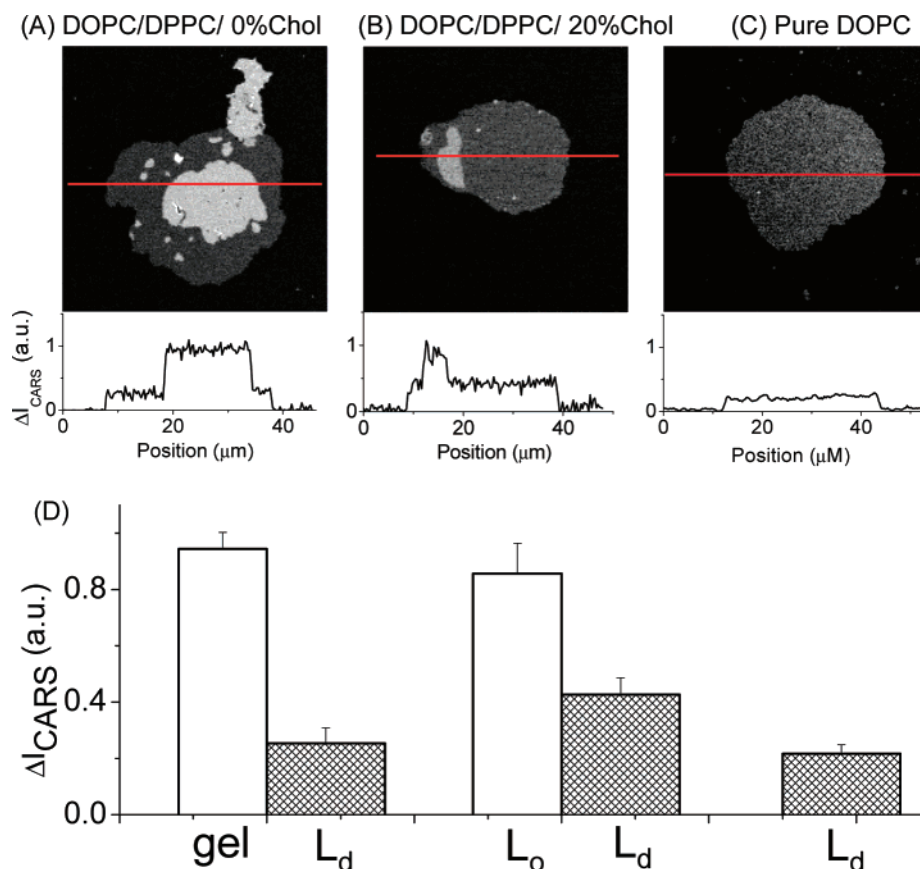


Figure 3. E-CARS images of the bilayer patches composed of (A) DOPC/DPPC (1:1), (B) DOPC/DPPC/cholesterol (4:4:2) in molar concentrations, and (C) pure DOPC. The intensity profiles along the red lines are shown below each image. (D) The values of ΔI_{CARS} for the gel, L_o , and L_d domains in sample (A), (B), and (C). In each sample, four patches were measured to obtain the error bars.

Meanwhile, the resonant CARS intensity from the L_d phase in the DOPC/DPPC/20% cholesterol bilayer was higher than that from the L_d phase of the pure DOPC bilayer (Figure 3C), whereas the CARS intensity from the L_d phase in the DOPC/DPPC bilayer was comparable to that from the L_d phase of the pure DOPC bilayer. These results provide direct evidence that cholesterol increases the solubility between DPPC and DOPC. In accordance, fluorescence imaging studies showed that phase segregation in GUVs disappeared when the cholesterol percentage exceeded a certain value.²²

Conclusions

CARS microscopy has been used for label-free imaging of lipid domains in single bilayers based on the different lipid packing density in the solid (S_o), liquid-ordered (L_o), and liquid-disordered (L_d) thermodynamic states. By using epidetection to suppress the nonresonant background, we observed clear contrast in CARS images of supported bilayer patches with coexisting domains. This method provides a way to determine the lipid phase diagram of unilamellar lipid bilayers without any labeling. In combination with two-photon-excited fluorescence that can be performed on the same CARS microscope,² it can be applied to study the interaction of specific proteins or peptides with lipid domains in a supported bilayer. Furthermore, this method can be potentially used for direct visualization of macroscopic domains, for example, aggregated rafts,²³ in the plasma membrane of live cells.

Acknowledgment. This work is supported by a National Science Foundation Grant (0416785-MCB). The authors thank Dr. Haifeng Wang for his help in the CARS imaging experiment.

References and Notes

- (1) Cheng, J. X.; Xie, X. S. *J. Phys. Chem. B* **2004**, *108*, 827.
- (2) Cheng, J. X. *Appl. Spectrosc.* **2007**, *61*, 197A.
- (3) Müller, M.; Zumbusch, A. *ChemPhysChem* **2007**, *8*, 2156.
- (4) Shen, Y. R. *The Principles of Nonlinear Optics*; John Wiley and Sons Inc.: New York, 1984.
- (5) Cheng, J. X.; Jia, Y. K.; Zheng, G.; Xie, X. S. *Biophys. J.* **2002**, *83*, 502.
- (6) Wurpel, G. W. H.; Schins, J. M.; Müller, M. *J. Phys. Chem.* **2004**, *108*, 3400.
- (7) Potma, E. O.; Xie, X. S. *ChemPhysChem* **2005**, *6*, 77.
- (8) Li, L.; Wang, H.; Cheng, J. X. *Biophys. J.* **2005**, *89*, 3480.
- (9) Lentz, B. R.; Barenholz, Y.; Thompson, T. E. *Biochemistry* **1976**, *15*, 4529.
- (10) Ipsen, J. H.; Karlström, G.; Mourtsen, O. G.; Wennerström, H.; Zuckermann, M. J. *Biochim. Biophys. Acta* **1987**, *905*, 162.
- (11) Tristram-Nagle, S.; Liu, Y.; Legleiter, J.; Nagle, J. F. *Biophys. J.* **2002**, *83*, 3324.
- (12) Costigan, S. C.; Booth, P. J.; Templer, R. H. *Biochim. Biophys. Acta* **2000**, *1468*, 41.
- (13) Staneva, G.; Seigneuret, M.; Koumanov, K.; Trugnan, G.; Angelova, M. I. *Chem. Phys. Lipids* **2005**, *136*, 55.
- (14) Kaizuka, Y.; Groves, J. T. *Biophys. J.* **2004**, *86*, 905.
- (15) Hamai, C.; Yang, T.; Kataoka, S.; Cremer, P. S.; Musser, S. M. *Biophys. J.* **2006**, *90*, 1241.
- (16) Czajkowsky, D. M.; Huang, C.; Shao, Z. *Biochemistry* **1995**, *34*, 12501.
- (17) Veatch, S. L.; Keller, S. L. *Biophys. J.* **2003**, *85*, 3074.
- (18) Volkmer, A.; Cheng, J. X.; Xie, X. S. *Phys. Rev. Lett.* **2001**, *87*, 023901.
- (19) Potma, E. O.; Xie, X. S. *J. Raman Spectrosc.* **2003**, *34*, 642.
- (20) Lotem, H.; Lynch, R. T. J.; Bloembergen, N. *Phys. Rev. A* **1976**, *14*, 1748.
- (21) Nagle, J. F.; Tristram-Nagle, S. *Curr. Opin. Struct. Biol.* **2000**, *10*, 474.
- (22) Scherfeld, D.; Kahya, N.; Schwill, P. *Biophys. J.* **2003**, *85*, 3758.
- (23) Edidin, M. *Annu. Rev. Biophys. Biomol. Struct.* **2003**, *32*, 257.